An Energy Shaping Exoskeleton Controller for Human Strength Amplification

Gray Cortright Thomas and Robert D. Gregg

***Abstract*— In this work, we introduce a novel approach to assistive exoskeleton (or powered orthosis) control which avoids needing task and gait phase information. Our approach is based on directly designing the Hamiltonian dynamics of the target closed-loop behavior, shaping the energy of the human and the robot. Relative to previous energy shaping controllers for assistive exoskeletons, we introduce ground reaction force and torque information into the target behavior definition, reformulate the kinematics so as to avoid explicit matching conditions due to under-actuation, and avoid the need to switch between swing and stance energy shapes. Our controller introduces new states into the target Hamiltonian energy that represent a virtual second leg that is connected to the physical leg using virtual springs. The impulse the human imparts to the physical leg is amplified and applied to the virtual leg, but the ground reaction force acts only on the physical leg. A state transformation allows the proposed control to be available using only encoders, an IMU, and ground reaction force sensors. We prove that this controller is stable and passive when acted on by the ground reaction force and demonstrate the controller's strength amplifying behavior in a simulation. A linear analysis based on small signal assumptions allows us to explain the relationship between our tuning parameters and the frequency domain amplification bandwidth.**

I. Introduction

Recent advances in exoskeleton technology have resulted in a class of light-weight assistive lower-body exoskeletons that can reduce the muscle effort [1] or metabolic cost of locomotion [2]–[5]. These systems are a departure from the better known humanoid-like lower-body exoskeletons (e.g. HAL [6], ATLANTE [7], ReWalk [8], or Mina v2 [9]) in that they are designed not to impose kinematics but rather to be back-driven by the users, providing assistive torque to augment a human that remains in direct control of the limb kinematics. But a lack of control strategies that allow these devices to transition between the various tasks (such as walking at different speeds, over ramps, up stairs, etc.) is one of the key factors keeping them from practical application [10]. These transitions are critical for assisting people in activities of daily living (ADLs) which feature short bouts of walking on the order of 30 seconds [11].

Control strategies that are designed to reduce metabolic cost of transport typically exploit the periodic nature of treadmill walking experiments to simplify the problem, but these approaches do not scale easily to handle more realistic ADLs that are not truly periodic. For example, timing-based control approaches play forward a desired trajectory based on detection of periodic events such as heel-strikes [3], sometimes superimposed with virtual mechanical impedance [2]. Adaptive oscillator strategies use nonlinear control to fit oscillator outputs to the periodic motion of joint angles, and from oscillator states produce control signals [12]. Phase estimation strategies use a data-driven model and an internal dynamic state to more accurately track human motions and apply phase-based torque profiles [13], [14]. All these types of controllers require alterations to enable transitions between gait modes like level ground walking and stair ascent (or even more subtle changes like walking fast or walking slow). Machine learning systems for gait classification take information from previous steps to estimate the mode for the upcoming step. However this requires a significant quantity of training data for each gait mode, and experiments to obtain this data are expensive. Thus, the long-term scalability of the periodic motions with task classification strategies are dubious unless supplemented by a backup plan that works acceptably in the many tasks that were not part of the training set. Controllers have also avoided task dependence or the periodicity assumption using convenient relationships—delayed output feedback of thigh angle as a hip torque approximation, for example [15]—but such relationships may not necessarily scale to other exoskeletons and task sets.

An emerging approach called "Energy shaping" [16], [17] offers to remove the restriction to periodic behavior and allow freer transitions between tasks, but still cannot reproduce scaled human torques for any activity. Similar to the way integral admittance shaping assigns a desired linear behavior in closed-loop [18], energy shaping assigns a nonlinear closed-loop behavior. The paradigm of energy shaping is designed after passive dynamic walking systems from the study of humanoid robots. In these systems, energy shaping of the natural walking dynamics is capable of making a robot on level ground behave like a passive dynamic walker going down a slope [19]. And by analogy, the purpose of energy shaping in exoskeletons has been to alter the natural dynamics such that locomotion is easier in general (and independent of, for example, the speed, ramp angle, step length, etc.).

Energy shaping works by assigning a new target energy to a mechanical model of the human-and-exoskeleton system, typically in the sagittal plane, and backing out the control torques necessary to make the closed loop system obey the dynamics that would arise from the target energy according to classical (Lagrangian/Hamiltonian/Routhian) mechanics.

This work was supported by the National Science Foundation under Award Numbers 1949869 and 1953908.

G. C. Thomas and R. D. Gregg are with the Division of Electrical and Computer Engineering and the Robotics Institute, University of Michigan, Ann Arbor, MI 48109, USA. (Correspondence: {gcthomas, rdgregg}@umich.edu)

The framework requires the target energy to satisfy "matching conditions" for under-actuated systems (i.e. the existence of a control law). Previous work has solved the matching conditions for fully actuated chains beginning at the foot (including when the foot contact state is unknown [20]), introduced ground reaction force scaling to avoid abrupt torque changes between stance and swing controllers [21], and established energy shaping as a viable paradigm for assistance that is helpful across multiple tasks through optimization over the parameters of the target energy [22], [23]. However, as they exist now, energy shaping controllers for exoskeletons do not support amplification of human torques relative to other system inputs like the ground reaction force.

Controllers that aim to amplify human strength exist outside the context of lightweight lower-body exoskeletons. For example, the human extender structure [24] amplifies strength in a fixed-based manipulator context by measuring both the force the human applies to the robot and the force the robot applies to the environment, using error feedback to ensure the environmental force is some multiple of the human force. Results on simple 1-DOF systems have shown that it is also possible to achieve amplification using force/torque sensors between the exoskeleton and the wearer [25], [26], but this sensor configuration is impractical for lightweight assistive devices.

In this paper we 1) propose a novel energy-shaping controller that uses ground reaction force information to amplify human strength without task knowledge or special parameter tuning, 2) show that the resulting closed loop system is stable and passive at the environment input, and 3) validate this controller's stable amplification of human strength using a simulation. More specifically, we hypothesize that H1) the novel energy-shaping controller will converge toward a constant rate of amplification of human strength in steady state, H2) the controller will not need human torque measurements, joint acceleration feedback, or inertia reduction in the target energy, H3) the controller is independently passive at the environment port, and H4) the controller bandwidth can be tuned using a frequency domain interpretation of the controller. We demonstrate our controller's amplification behavior in a 2D rigid body simulation.

II. Modeling and Control

We consider an idealized assistive exoskeleton system in 2D on a single leg of a person. This exoskeleton actuates the hip, knee, and ankle joints through a torque command and measures the 2D ground reaction force/torque vector, joint angles, and global angle and acceleration of the hip. The torque commands are assistive, acting in concert with human joint torques. The global information available for the hip link is a noiseless representation of what could be inferred from a thigh-mounted IMU. And the other measurements are representations of what could be calculated from joint encoders and a force/torque sensor between the person's foot and the ground. We define the kinematics of the human/robot model using global angle coordinates as shown in Fig. 1

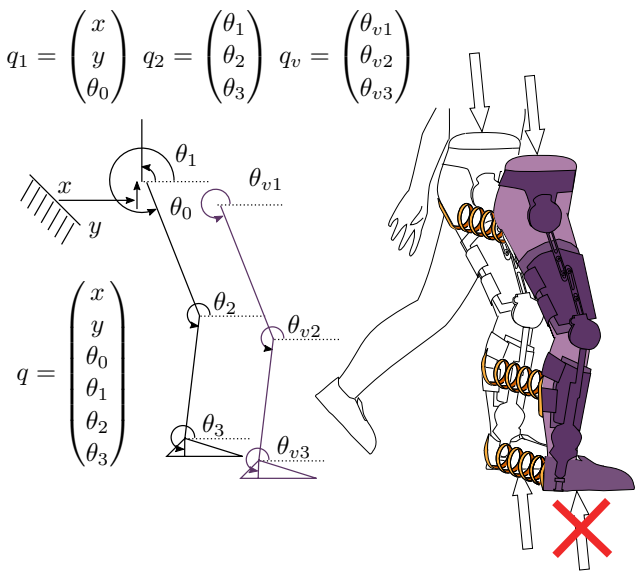

Fig. 1. **Illustration of the virtual spring and inertia system**—the proposed controller shapes the energy of the target system, the augmented human leg, to include an extra kinetic energy term similar to that of a second virtual copy of the leg floating to the side of the true leg. The controller additionally adds potential energy that can be visualized as angular springs connecting the virtual leg segments to the true leg segments. The fundamental mechanism by which the controller amplifies human strength is denying the virtual leg a copy of the ground reaction forces and the gravity vector, while allowing it a copy of every other force acting on the true leg system. This configuration allows human joint torques to actuate both the real and virtual legs, magnifying their power, while ground reaction forces act only on the true leg. Once the virtual springs reach equilibrium, the human will be providing only half the torque necessary to resist the ground reaction force, with the exoskeleton providing the rest. Other amplification ratios can be attained by changing the mass of the virtual leg to be larger or smaller than the true leg.

(alongside coordinate definitions for the virtual leg our controller will be simulating).

The goal of our modeling is to first describe the 6-DOF dynamics of the floating leg system, and then extract the smaller 3-DOF leg system that we will alter using energy shaping. The goal of our control is to design a target Hamiltonian system for this 3-DOF system that has the strength amplification property we seek, and which is also passive at the 3 ports of the 3-DOF system: the human joint angle/joint torque port, the human hip position/hip forces port, and the foot position/ground reaction force port.

The actuated leg is only a small part of the entire human-robot system, but we will model it as an independent port-Hamiltonian system connected to the rest of the person by an interaction port. To form this model, we will first consider the actuated leg as a floating-base system, and then apply a position constraint at the hip. However, the acceleration of this hip and the states of the floating base joints will remain as inputs to the system. From this floating leg model, we will extract the dynamics of the three actuated joints. We will then be able to re-express these 3-DOF dynamics as resulting from the fixed-base 3-joint leg system's Hamiltonian with an inertial input representing the influence of the hip's acceleration. We will then perform our energy shaping on the

fully controllable 3-joint system, rather than on the floating leg model, which trivializes the matching conditions and also provides the prototype for the dynamics of the virtual leg system that our target Hamiltonian will add.

A. The 6-DOF Floating Leg Model

We first consider the equations of motion for the 2D floating leg system. We represent them using the standard robot equation with four interaction ports: 1) between the floating hip and the rest of the person, 2) between the foot and the ground, 3) between the human neuromusular system and the inertia of the leg, and 4) between the robot actuators and the inertia of the leg. The robot equation is then

$$M\ddot{q} + B\dot{q} + g + J_e^T f_e + J_b^T f_b = S(\tau_H + \tau_R), \quad (1)$$

where M is the mass matrix, $q \in \mathbf{R}^6$, $\dot{q}$, and $\ddot{q}$ are the generalized joint angles, velocities, and accelerations, B is the Coriolis matrix, and g is the gravitational torque resulting from the gravitational potential function $G(q)$ such that $g = \nabla_q G(q)$. The first two port interactions are represented by J_b and f_b—the Jacobian and force for the port connecting the leg to the hip (labeled b for being the base of the serial kinematic chain of the leg), and J_e and f_e—the Jacobian and force for the port where the foot interacts with the ground, labeled with e for environment. The vector τ_H represents the actuation torques from the human neuromusuclar system, and τ_R represents the actuation torques from the robot's actuators. The matrix $S \in \mathbf{R}^{6\times 3}$ represents the under-actuation structure in the global angle coordinate system.

$$S = \begin{pmatrix} S_1 \\ S_2 \end{pmatrix}, \text{where } S_1 = \begin{pmatrix} 0 & 0 & 0 \\ 0 & 0 & 0 \\ 1 & 1 & 1 \end{pmatrix}, \; S_2 = \begin{pmatrix} 1 & 1 & 1 \\ 0 & 1 & 1 \\ 0 & 0 & 1 \end{pmatrix}. \quad (2)$$

In preparation for separating out the floating base dynamics, we subdivide $q = \begin{pmatrix} q_1^T & q_2^T \end{pmatrix}^T$ as shown in Fig. 1, with the floating base joints represented by $q_1 \in \mathbf{R}^3$ and the global thigh, shank, and foot angles by $q_2 \in \mathbf{R}^3$. Our robot equation becomes a block matrix equality:

$$\begin{pmatrix} M_{11}(q_1) & M_{12} \\ M_{12}^T & M_{22}(q_2) \end{pmatrix} \begin{pmatrix} \ddot{q}_1 \\ \ddot{q}_2 \end{pmatrix} + \begin{pmatrix} B_{11} & B_{12} \\ B_{21} & B_{22} \end{pmatrix} \begin{pmatrix} \dot{q}_1 \\ \dot{q}_2 \end{pmatrix} + \begin{pmatrix} g_1 \\ g_2 \end{pmatrix} + \begin{pmatrix} J_{e1}^T \\ J_{e2}^T \end{pmatrix} f_e + \begin{pmatrix} I \\ 0 \end{pmatrix} f_b = S(\tau_H + \tau_R). \quad (3)$$

B. The 3-DOF Leg Model

The constrained dynamics of the lower three joints are evident in (3). We represent them as resulting from a fully controllable lower-dimensional Hamiltonian system with inputs from 1) the position, velocity, and acceleration of the hip, 2) the ground reaction force at the foot, 3) the joint torques of the human, and 4) the joint torques of the exoskeleton. That is, we flip the causality of the hip port relative to the previous model, taking position (and its derivatives) instead of torque as the input. From the second row of the separated robot equation,

$$M_{22}\ddot{q}_2 + B_{22}\dot{q}_2 + g_2 + J_{e2}^T f_e + M_{12}^T \ddot{q}_1 + B_{21}\dot{q}_1 = S_2(\tau_H + \tau_R). \quad (4)$$

Note that S_2 is nonsingular.

This behavior can be represented as resulting from the following Hamiltonian system defined by position q_2 and momentum $p_2 = M_{22}\dot{q}_2$, with a mass matrix that depends on both q_2 and q_1, and with an input τ',

$$\mathcal{H} = \frac{1}{2} p_2^T M_{22}^{-1} p_2 + G_2(q_2), \quad (5)$$

$$\dot{q}_2 = \nabla_{p_2} \mathcal{H} = M_{22}^{-1} M_{22} \dot{q}_2, \quad (6)$$

$$\dot{p}_2 = -\nabla_{q_2} \mathcal{H} + \tau' = -\nabla_{q_2} \left[\frac{1}{2} p_2^T M_{22}^{-1} p_2 \right] - g_2 + \tau', \quad (7)$$

where $G_2(q_2)$ represents the gravitational potential energy due to the actuated leg joints, $G_2(q_2) = G(q) - G((q_1^T \; 0)^T)$, such that $\nabla_{q_2} G_2(q_2) = g_2$. Note that, in the global angle formulation of the kinematics, $\nabla_{q_1}[G(q) - G((q_1^T \; 0)^T)] = 0$. In the form of a robot equation, this becomes

$$M_{22}\ddot{q}_2 + \dot{M}_{22}\dot{q}_2 + \nabla_{q_2} \left[\frac{1}{2} p_2^T M_{22}^{-1} p_2 \right] + g_2 = \tau'. \quad (8)$$

To use this Hamiltonian system to describe the dynamics of the hip, knee, and ankle joints, we calculate the τ' necessary to make the two equations of motion agree:

$$\tau' = \cancel{\left(\dot{M}_{22}\dot{q}_2 + \nabla_{q_2} \left[\frac{1}{2} p_2^T M_{22}^{-1} p_2 \right] - B_{22}\dot{q}_2 \right)} - M_{12}^T \ddot{q}_1 - B_{21}\dot{q}_1 + S_2(\tau_H + \tau_R) - J_{e2}^T f_e. \quad (9)$$

In this expression, the first term compares two Coriolis terms, and is guaranteed to result in a skew symmetric matrix times $\dot{q}_2$. However, in a global angle coordinate system, this term cancels. What remains are the dynamic influences from the motion of the base joints, and the inputs from the human musculature, the robot actuators, and the ground contact. Since S_2 is invertible, this 3-DOF system is fully actuated.

C. A Target Energy for the 3-DOF Leg System

With these preliminaries, we can now introduce our target energy shape and dynamical system behavior. Our target system introduces two new state vectors: $q_v \in \mathbf{R}^3$ represents the angles of the virtual robot, and $p_v \in \mathbf{R}^3$ represents the momenta corresponding to the virtual inertia. The target Hamiltonian is as follows,

$$\mathcal{H}' = \frac{1}{2} p_2^T M_{22}^{-1} p_2 + \frac{1}{2}(q_2 - q_v)^T K_v (q_2 - q_v) + \frac{1}{2} p_v^T M_v^{-1} p_v + G_2(q_2), \quad (10)$$

where the newly introduced $K_v = K_v^T \succeq 0 \in \mathbf{R}^{3\times 3}$ represents the virtual spring stiffness, and the altered mass matrix $M_v = (\alpha - 1)M_{22}$ will eventually be responsible for defining the steady state amplification ratio $\alpha > 1$ between human and environmental forces. Note that both M and M_v depend on both q_2 and potentially on q_1 as well, but that M_v does not depend on q_v. The momentum of the virtual system still follows the standard definition $p_v = M_v \dot{q}_v$.

This definition of a virtual system that is mass-matrix coupled to the robot system results in complex Coriolis-like terms. However this complexity is worthwhile, since

the alternative of having the virtual system control its own mass matrix could lead to singularities like knee reversal that would be hidden from the user.

When specifying a target dynamic, we emphasize the importance of also specifying the relationship this new system energy will have to the inputs to the system. This information is not contained in the definition of a target Hamiltonian alone, but in the definition of an external torque vector similar to τ' in our reduced-order system. Since we have augmented the state, our new system will have an external torque $\tau_v \in \mathbf{R}^6$. By design, this system is fully actuated, so we do not need to solve matching conditions. We define the state vector as

$$x = \begin{pmatrix} q_2^T & q_v^T & p_2^T & p_v^T \end{pmatrix}^T, \tag{11}$$

and by the classical Hamiltonian equations of motion,

$$\dot{x} = \begin{pmatrix} 0 & 0 & I & 0 \\ 0 & 0 & 0 & I \\ -I & 0 & 0 & 0 \\ 0 & -I & 0 & 0 \end{pmatrix} \nabla_x \mathcal{H} + \begin{pmatrix} 0 & 0 \\ 0 & 0 \\ I & 0 \\ 0 & I \end{pmatrix} \tau_v. \tag{12}$$

We define the virtual external torque

$$\tau_v = \begin{pmatrix} -M_{12}^T \ddot{q}_1 - B_{21}\dot{q}_1 + S_2\tau_H - J_{e2}^T f_e - D_v(\dot{q}_2 - \dot{q}_v) \\ (\alpha - 1)\left[-M_{12}^T \ddot{q}_1 - B_{21}\dot{q}_1 + S_2\tau_H\right] + D_v(\dot{q}_2 - \dot{q}_v) \end{pmatrix}, \tag{13}$$

where the new matrix D_v applies linear damping to the virtual spring behavior. Let us introduce a variable γ_H to abbreviate the influence of the human, including both the direct torques of the leg and the inertial effects of human-directed hip acceleration and velocity,

$$\gamma_H = -M_{12}^T \ddot{q}_1 - B_{21}\dot{q}_1 + S_2\tau_H. \tag{14}$$

Theorem 1 (Environment-Side Passivity): For the environmental port described by the generalized velocity $\dot{x}_e = -J_{e2}\dot{q}_2$ and the generalized force f_e, $\mathcal{H}'(q_2, p_2, q_v, p_v)$ is an energy storage function which satisfies $\dot{\mathcal{H}}' \leq f_e^T \dot{x}_e$ in the condition where this port (with the ground reaction force as the input and the foot velocity as the output) is the only input to the system.

Proof: Considering the net energy into the system,

$$\dot{\mathcal{H}}' = \begin{pmatrix} \dot{q}_2^T & \dot{q}_v^T \end{pmatrix} \tau_v, \tag{15}$$

$$= \dot{q}_2^T[\gamma_H - J_{e2}^T f_e] + (\alpha - 1)\dot{q}_v^T \gamma_H - D\|\dot{q}_2 - \dot{q}_v\|^2, \tag{16}$$

and taking γ_H as zero as per the condition,

$$\dot{\mathcal{H}}' = -\dot{q}_2[J_{e2}^T f_e] - D\|\dot{q}_2 - \dot{q}_v\|^2$$
$$= f_e^T \dot{x}_e - D\|\dot{q}_2 - \dot{q}_v\|^2 \leq f_e^T \dot{x}_e \tag{17}$$

■

Note that, if the virtual spring reaches equilibrium, then this system will satisfy the relationship $\dot{q}_2 = \dot{q}_v$, in which case the energy change simplifies to

$$\dot{\mathcal{H}}'|_{\dot{q}_2 = \dot{q}_v} = \alpha \dot{q}_2^T \gamma_H - \dot{q}_2^T [J_{e2}^T f_e], \tag{18}$$

which highlights the way this target system prioritizes all inputs other than the environmental input, causing them to add α times as much energy to the system.

D. The Energy-Shaping Control Law

From this definition of the target behavior, we can back out the joint torque necessary to make it happen, and re-write it in terms of only *available* signals. Given our sensor setup, we assume that f_e is measured, and that an IMU provides a reliable estimate of $\ddot{q}_1$. This means that $-M_{12}^T \ddot{q}_1 - B_{21}\dot{q}_1$ is available. We can calculate the robot torque in terms of the state vector.

The q_2 dynamics of the original system are

$$M_{22}\ddot{q}_2 + b_2 + g_2 = \gamma_H + S_2\tau_R - J_{e2}^T f_e, \tag{19}$$

where

$$b_2 = \dot{M}_{22}\dot{q}_2 + \nabla_{q_2}\left[\frac{1}{2} p_2^T M_{22}^{-1} p_2\right]. \tag{20}$$

And for the target system, we have

$$M_{22}\ddot{q}_2 + b_2 + g_2 + \nabla_{q_2}\left[\frac{1}{2} p_v^T M_v^{-1} p_v\right] +$$
$$D_v(\dot{q}_2 - \dot{q}_v) + K_v(q_2 - q_v) = \gamma_H - J_{e2}^T f_e. \tag{21}$$

Subtracting the two equations allows us to solve for $S_2\tau_R$, as

$$S_2\tau_R = -\nabla_{q_2}\left[\frac{1}{2} p_v^T M_v^{-1} p_v\right] - D_v(\dot{q}_2 - \dot{q}_v) - K_v(q_2 - q_v). \tag{22}$$

To finish specifying the control law, we restate the dynamics of the virtual momentum,

$$\dot{p}_v + D_v(\dot{q}_v - \dot{q}_2) + K_v(q_v - q_2) = (\alpha - 1)\gamma_H, \tag{23}$$

or, expanding the momentum derivative,

$$(\alpha - 1)\dot{M}_{22}\dot{q}_v + (\alpha - 1)M_{22}\ddot{q}_v + D_v(\dot{q}_v - \dot{q}_2) + K_v(q_v - q_2) = (\alpha - 1)\gamma_H. \tag{24}$$

E. Amplification Relationship in Equilibrium (H1)

To validate H1, that the novel energy-shaping controller will converge toward a constant rate of amplification of human strength in steady state, we can solve these dynamics for zero velocity and acceleration conditions.

Theorem 2 (Amplification): Any equilibrium satisfying $\dot{q} = \ddot{q} = 0_6$, $\dot{q}_v = \ddot{q}_v = 0_3$ also satisfies the amplification law $\tau_R = (\alpha - 1)\tau_H$.

Proof: The equilibrium simplifies (22),

$$S_2\tau_R = -K_v(q_2 - q_v) = K_v(q_v - q_2), \tag{25}$$

and the q_v dynamics in (24),

$$K_v(q_v - q_2) = (\alpha - 1)S_2\tau_H. \tag{26}$$

And thus

$$S_2\tau_R = (\alpha - 1)S_2\tau_H. \tag{27}$$

Since the matrix S_2 is invertible,

$$\tau_R = (\alpha - 1)\tau_H. \tag{28}$$

■

Note that in this equilibrium condition, (4) becomes

$$g_2 + J_{e2}^T f_e = S_2(\tau_H + \tau_R) = \frac{\alpha}{\alpha - 1} S_2\tau_R, \tag{29}$$

so our control law is indirectly compensating gravity.

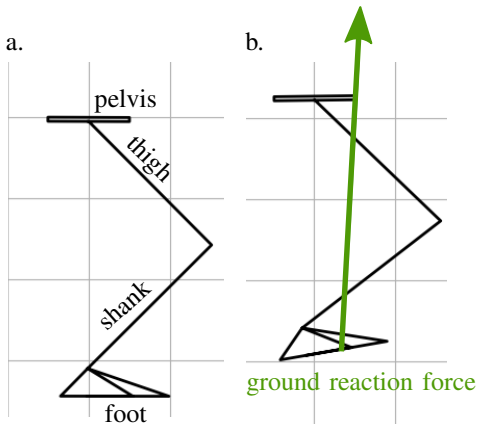

Fig. 2. **Simulation Visualization.** The initial configuration (a) is perturbed by a ground reaction force. A dynamic simulation featuring a spring-like human behavior—assisted by our exoskeleton control torques—determines the amount of deflection in the kinematics of the leg (b).

F. State Transformation and Availability of the Control (H2)

It is practically important that the controller will not require unavailable human torque measurements, or joint acceleration feedback, for which we do not have sensors. As written so far, the robot torque command in (22) is available, but the dynamic update that determines $\ddot{q}_v$ is not. Normalizing (24) by $\alpha - 1$, we see

$$M_{22}\ddot{q}_v + \dot{M}_{22}\dot{q}_v + \frac{D_v(\dot{q}_v - \dot{q}_2) + K_v(q_v - q_2)}{\alpha - 1} = \gamma_H, \tag{30}$$

which still depends on the unavailable τ_H.

We can get around this by introducing a new state variable,

$$q_\Delta = q_v - q_2, \tag{31}$$

which follows a dynamic equation obtained by subtracting (21) from (30):

$$M_{22}(\ddot{q}_v - \ddot{q}_2) + \left(\dot{M}_{22}\dot{q}_v - b_2 - \nabla_{q_2}\left[\frac{1}{2}p_v^T M_v^{-1} p_v\right]\right) + \frac{\alpha}{\alpha - 1}\left(D_v(\dot{q}_v - \dot{q}_2) + K_v(q_v - q_2)\right) = J_{e2}^T f_e + g_2, \tag{32}$$

which cancels γ_H, yielding available $\ddot{q}_\Delta$ dynamics,

$$M_{22}\ddot{q}_\Delta + \frac{\alpha D_v}{\alpha - 1}\dot{q}_\Delta + \frac{\alpha K_v}{\alpha - 1}q_\Delta = J_{e2}^T f_e + g_2 - b_\Delta, \tag{33}$$

$$\text{where } b_\Delta = \dot{M}_{22}\dot{q}_v - b_2 - \nabla_{q_2}\left[\frac{1}{2}p_v^T M_v^{-1} p_v\right]. \tag{34}$$

Here, the new term b_Δ represents an amalgamation of Coriolis terms unique to our situation of two systems sharing the mass matrix M_{22} that is influenced only by one of their configuration vectors. Note that the dynamics of $\ddot{q}_\Delta$ in (33) are driven by only the foot's force/torque sensors signal, gravity, and the Coriolis term, b_Δ.

G. Low Pass Filter Interpretation

The structure of (33) is highly suggestive of a low pass filter system. With matrix fractions indicating right multiplication by the inverse of the denominator, we could approximate the robot torques as resulting from this multi-input multi-output low pass filter system under the assumption of a constant mass matrix:

$$\overbrace{S_2\tau_R(s)}^{\text{exo torque is}} \approx \overbrace{\frac{\frac{\alpha-1}{\alpha}(D_v s + K_v)}{\frac{\alpha-1}{\alpha}M_{22}s^2 + D_v s + K_v}}^{\text{scaled and low-pass filtered}} \Big[\overbrace{J_{e2}^T f_e}^{\text{GRF and}} + \overbrace{g_2}^{\text{gravity}} \overbrace{- b_\Delta}^{\text{plus some unusual Coriolis terms}} \Big](s) - \nabla_{q_2}\left[\frac{1}{2}p_v^T M_v^{-1} p_v\right](s). \tag{35}$$

This expression is useful in that it offers an intuitive explanation for what this control does: The ground reaction force is mapped to joint torques using the manipulator Jacobian J_{e2}, low pass filtered, scaled by $1 - 1/\alpha$, and applied to the joints. By doing this, the exoskeleton attempts to support a significant portion of the load from the reaction force. When the human pushes against the ground in steady state, an equilibrium is reached whereby the human applies $1/\alpha \cdot (J_{e2}^T f_e + g_2)$ and the exoskeleton $(1 - 1/\alpha) \cdot (J_{e2}^T f_e + g_2)$. Meanwhile, the steady state inclusion of $(1 - 1/\alpha)b_\Delta$ in the robot torque serves to average out the Coriolis effects between the virtual and the physical leg.

The linear interpretation also reveals the relationship between the controller's frequency domain amplification bandwidth and the tuning parameters K_v and D_v. This bandwidth relationship is empirically useful in avoiding instabilities related to discrete time implementation.

III. Methods of Validation in Simulation

We build our dynamic simulation environment using the DART multibody dynamics engine in Python. In the simulation, the human joint torques act as joint spring-damper systems, and this includes the 3 degrees of freedom that represent the floating base (q_1). The simulation excites the system with an external force that approximates a ground reaction force (Fig. 2). A simple geometric law determines the center of pressure and direction of force, and the magnitude follows a 1 Hz periodic pulse trajectory in time. Due to this external force, the simulated leg flexes periodically. For ease of interpreting the results, we use an amplification controller with amplification rate $\alpha = 2$, such that the human torque and the exoskeleton torque are equal in equilibrium.

To explore the behavior of the closed loop system, we simulated two conditions in particular. In the first 'damped human' condition, the joint damping parameters are set to large values such that the leg flexes without significant overshoot. In the second 'undamped knee' condition, the knee damping is set to zero. This results in clear underdamped oscillations[1] in response to the perturbation from the simulated ground reaction force pulses.

[1]But not persistent oscillations, as the rest of the human joints will still remove energy.

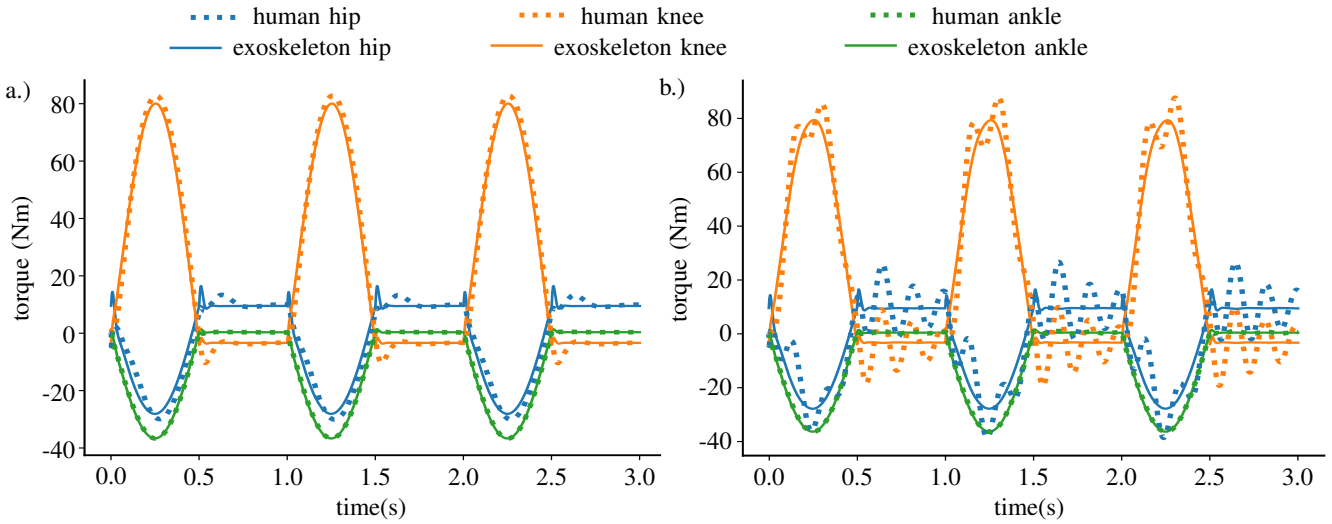

Fig. 3. **Results of the two simulation experiments with exoskeleton assistance factor 2**—Damped human condition (a) and under-damped knee condition (b). Since the amplification factor is 2, the human and exoskeleton joint torque contributions should be equal. As expected, this ideal behavior is maintained in the damped human condition. In this case, human joint torques work to compensate for the ground reaction force and gravity, and the exoskeleton correctly matches these contributions. In the under-damped knee condition, there is a human-driven oscillation, which results in human-versus-inertia forces. Since the exoskeleton does not modify the inertia of the human's leg, these oscillations appear only in the human torques. (That is, the exoskeleton no longer closely tracks the human joint torques for this reason.)

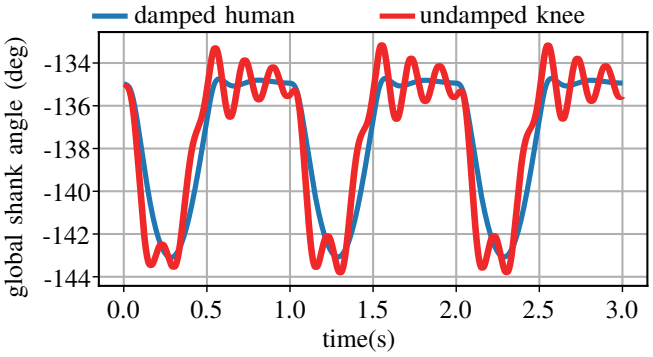

Fig. 4. **"Human Oscillation" of the global shank angle.** Subsequent pulses of ground reaction force serve to excite an under-damped oscillation between the inertia of the shank and foot and the simulated knee spring that is unique to the undamped knee experimental condition. This critical feature of Simulation 2 serves to highlight the *lack* of human strength amplification during such behaviors, which has both advantages and disadvantages for the task-invariant assistive exoskeleton use case.

The purpose of these two tests is to highlight two fundamental modes of interaction: human musculoskeletal torques vs. ground reaction forces and human musculoskeletal torques vs. human leg inertia. The first interaction is representative of the stance phase of walking, where human joint torques resist the ground reaction force to prevent the leg from collapsing. The second is akin to the behavior in swing phase, where the muscle torques work primarily against the inertia of the leg in order to achieve the next ground contact location.

IV. Simulation Results

The exoskeleton torques and human torques follow largely identical patterns for the first experiment (Fig. 3.a). Between 0 and 0.5 seconds (as well as from 1-1.5 and 2-2.5 seconds), the leg is being forced by a ground reaction force and the exoskeleton is providing torque that directly assists the human in resisting this external force. Between .5 and 1 second (also 1.5-2 and 2.5-3 seconds) the ground reaction force is zero, and the exoskeleton is primarily performing a partial gravity compensation to lift the dangling lower leg relative to the hip.

During the second simulation, the human hip and knee torques have an oscillatory component at approximately 1.5 Hz due to the oscillating knee position; however, the exoskeleton torque is essentially unchanged from the previous test (Fig. 3.b). The presence of the periodic signal is easily explained by the under-damped motions of the shank and foot segments in the second test (Fig. 4).

In both tests, the exoskeleton torques display a small, quick, under-damped transient at the end of each pulse.

V. Discussion

The result of the first simulation indicates that our controller amplifies human strength without task knowledge, and the result of the second test adds the important caveat that this amplification ignores human-driven oscillation. This controller is ideally suited to assistance during stance, or in locomotion with minimal swing (such as slow jogging at a fast cadence). It is intuitive that resisting the ground reaction force is a broadly applicable strategy in stance phase while intentionally avoiding acceleration feedback limits performance in fast swing phases.

The actual "task-invariant performance" of the controller—or any quantification of human torque mimicry across a representative sample of activities of daily living—is still unknown. Our controller currently demonstrates

only task-agnostic assistance in a simplified example task, which reflects neither biofidelic mechanical impedance of the human in response to disturbances nor realistic nominal torque and angle trajectories. We hope to answer the question of task-invariance in our future work, once we resolve some lingering issues of dynamical consistency between the estimated accelerations, joint torques, and force plate data in our multi-task dataset.

The use of simultaneous amplification and kinetic reshaping (which would allow amplification of even human-driven oscillation) would require a more careful study of coupled stability than we have performed here. Kinetic reshaping introduces acceleration feedback. And our linear models suggest that kinetic reshaping is inherently non-passive.

The small under-damped transients in the exoskeleton torque are the result of our controller's finite bandwidth, and can be tuned with the K_v and D_v parameters. This is a critical degree of freedom for any practical implementation. Real systems have compliant human interfaces, time-discretization, time delay, and bandwidth limitations. And, by adjusting the finite amplification bandwidth, we can reduce the magnitude of the control signal at the frequencies where these effects are dominant.

To capture the potential of robotic exoskeletons to improve quality of life for people with weakened lower limb muscles, exoskeleton controllers need to allow for non-periodic and unpredictable activities of daily life. In this paper we have introduced a novel energy-shaping controller that is task-agnostic and capable of assisting the human joint torques in resisting ground reaction forces, but which leaves the swing dynamics of the leg unaltered aside from compensating gravity. And we have demonstrated that the controller is stable, is energetically passive with respect to the ground contact, and amplifies human impulse by a known amplification factor.

REFERENCES

[1] H. Zhu, C. Nesler, N. Divekar, V. Peddinti, and R. Gregg, "Design principles for compact, backdrivable actuation in partial-assist powered knee orthoses," *IEEE/ASME Transactions on Mechatronics*, 2021.

[2] L. M. Mooney, E. J. Rouse, and H. M. Herr, "Autonomous exoskeleton reduces metabolic cost of human walking during load carriage," *J. neuroengineering and rehabilitation*, vol. 11, no. 1, p. 80, 2014.

[3] J. Zhang, P. Fiers, K. A. Witte, R. W. Jackson, K. L. Poggensee, C. G. Atkeson, and S. H. Collins, "Human-in-the-loop optimization of exoskeleton assistance during walking," *Science*, vol. 356, no. 6344, pp. 1280–1284, 2017.

[4] J. Kim, G. Lee, R. Heimgartner, D. Arumukhom Revi, N. Karavas, D. Nathanson, I. Galiana, A. Eckert-Erdheim, P. Murphy, D. Perry, N. Menard, D. K. Choe, P. Malcolm, and C. J. Walsh, "Reducing the metabolic rate of walking and running with a versatile, portable exosuit," *Science*, vol. 365, no. 6454, pp. 668–672, 2019. [Online]. Available: https://science.sciencemag.org/content/365/6454/668

[5] G. S. Sawicki, O. N. Beck, I. Kang, and A. J. Young, "The exoskeleton expansion: improving walking and running economy," *J. neuroengineering and rehabilitation*, vol. 17, no. 1, pp. 1–9, 2020.

[6] K. Suzuki, G. Mito, H. Kawamoto, Y. Hasegawa, and Y. Sankai, "Intention-based walking support for paraplegia patients with robot suit hal," *Advanced Robotics*, vol. 21, no. 12, pp. 1441–1469, 2007.

[7] O. Harib, A. Hereid, A. Agrawal, T. Gurriet, S. Finet, G. Boeris, A. Duburcq, M. E. Mungai, M. Masselin, A. D. Ames, K. Sreenath, and J. W. Grizzle, "Feedback control of an exoskeleton for paraplegics: Toward robustly stable, hands-free dynamic walking," *IEEE Control Systems Magazine*, vol. 38, no. 6, pp. 61–87, 2018.

[8] G. Zeilig, H. Weingarden, M. Zwecker, I. Dudkiewicz, A. Bloch, and A. Esquenazi, "Safety and tolerance of the rewalk™ exoskeleton suit for ambulation by people with complete spinal cord injury: A pilot study," *The journal of spinal cord medicine*, vol. 35, no. 2, pp. 96–101, 2012.

[9] R. Griffin, T. Cobb, T. Craig, M. Daniel, N. van Dijk, J. Gines, K. Kramer, S. Shah, O. Siebinga, J. Smith, and P. Neuhaus, "Stepping forward with exoskeletons: Team IHMC's design and approach in the 2016 cybathlon," *IEEE Robotics Automation Magazine*, vol. 24, no. 4, pp. 66–74, 2017.

[10] T. Yan, M. Cempini, C. M. Oddo, and N. Vitiello, "Review of assistive strategies in powered lower-limb orthoses and exoskeletons," *Robotics and Autonomous Systems*, vol. 64, pp. 120–136, 2015.

[11] M. S. Orendurff, J. A. Schoen, G. C. Bernatz, A. D. Segal, and G. K. Klute, "How humans walk: bout duration, steps per bout, and rest duration." *J. Rehab. Research & Development*, vol. 45, no. 7, 2008.

[12] R. Ronsse, T. Lenzi, N. Vitiello, B. Koopman, E. Van Asseldonk, S. M. M. De Rossi, J. Van Den Kieboom, H. Van Der Kooij, M. C. Carrozza, and A. J. Ijspeert, "Oscillator-based assistance of cyclical movements: model-based and model-free approaches," *Med. & bio. engineering & computing*, vol. 49, no. 10, pp. 1173–1185, 2011.

[13] K. Seo, Y. J. Park, J. Lee, S. Hyung, M. Lee, J. Kim, H. Choi, and Y. Shim, "Rnn-based on-line continuous gait phase estimation from shank-mounted imus to control ankle exoskeletons," in *2019 IEEE 16th Int. Conf. on Rehab. Robotics (ICORR)*, pp. 809–815.

[14] I. Kang, P. Kunapuli, and A. J. Young, "Real-time neural network-based gait phase estimation using a robotic hip exoskeleton," *IEEE Trans. Med. Robotics and Bionics*, vol. 2, no. 1, pp. 28–37, 2019.

[15] B. Lim, J. Lee, J. Jang, K. Kim, Y. J. Park, K. Seo, and Y. Shim, "Delayed output feedback control for gait assistance with a robotic hip exoskeleton," *IEEE Trans. Robotics*, vol. 35, no. 4, pp. 1055–1062, 2019.

[16] G. Lv and R. D. Gregg, "Underactuated potential energy shaping with contact constraints: Application to a powered knee-ankle orthosis," *IEEE Trans. Control Systems Tech.*, vol. 26, no. 1, pp. 181–193, 2018.

[17] G. Lv, H. Zhu, and R. D. Gregg, "On the design and control of highly backdrivable lower-limb exoskeletons: A discussion of past and ongoing work," *IEEE Control Systems Magazine*, vol. 38, no. 6, pp. 88–113, 2018.

[18] U. Nagarajan, G. Aguirre-Ollinger, and A. Goswami, "Integral admittance shaping: A unified framework for active exoskeleton control," *Robotics and Autonomous Systems*, vol. 75, pp. 310–324, 2016.

[19] M. W. Spong, J. K. Holm, and D. Lee, "Passivity-based control of bipedal locomotion," *IEEE Robotics & Automation Magazine*, vol. 14, no. 2, pp. 30–40, 2007.

[20] J. Lin, G. Lv, and R. D. Gregg, "Contact-invariant total energy shaping control for powered exoskeletons," in *2019 American Control Conference (ACC)*, 2019, pp. 664–670.

[21] N. V. Divekar, J. Lin, C. Nesler, S. Borboa, and R. D. Gregg, "A potential energy shaping controller with ground reaction force feedback for a multi-activity knee-ankle exoskeleton," in *2020 8th IEEE RAS/EMBS International Conference for Biomedical Robotics and Biomechatronics (BioRob)*, 2020, pp. 997–1003.

[22] G. Lv, H. Xing, J. Lin, R. D. Gregg, and C. G. Atkeson, "A task-invariant learning framework of lower-limb exoskeletons for assisting human locomotion," in *2020 American Control Conference (ACC)*, 2020, pp. 569–576.

[23] J. Lin, N. V. Divekar, G. Lv, and R. D. Gregg, "Optimal task-invariant energetic control for a knee-ankle exoskeleton," *IEEE Control Systems Letters*, vol. 5, no. 5, pp. 1711–1716, 2021.

[24] H. Kazerooni and J. Guo, "Human extenders," *J. Dynamic Systems, Measurement, and Control*, vol. 115, no. 2B, pp. 281–290, 1993.

[25] B. He, G. C. Thomas, N. Paine, and L. Sentis, "Modeling and loop shaping of single-joint amplification exoskeleton with contact sensing and series elastic actuation," in *2019 American Control Conference (ACC)*, 2019, pp. 4580–4587.

[26] G. C. Thomas, J. M. Coholich, and L. Sentis, "Compliance shaping for control of strength amplification exoskeletons with elastic cuffs," in *2019 IEEE/ASME Int. Conf. Advanced Intelligent Mechatronics (AIM)*, July, pp. 1199–1206.